(Received 26 September 2025, Accepted 27 November 2025, Scheduled 17 December 2025)

Design of Cascaded Circular Ring Semicircular Cresent Shaped Multiband Antenna for UWB, WLAN, WiMAX and 5G Midband Applications

Chevala Rambabu[1], Kaza Srilakshmi[1], Vasudha V. Bolisetty[2], Udara Yedukondalu[3], and Kottapadikal V. Vineetha[4,*]

[1]*Department of Electronics and Communication Engineering Seshadri Rao Gudlavalleru Engineering College, Gudlavalleru, Krishna District, Andhra Prades 521356, India*
[2]*Department of ECE, Aditya University, Surampalem 533437, India*
[3]*Department of ECE, MVR College of Engineering and Technology, Paritala, Andhra Pradesh 521180, India*
[4]*Department of Electronics and Communication Engineering Koneru Lakshmaiah Education Foundation, Vaddeswaram, Guntur 522502, India*

ABSTRACT: In this paper, we report a cascaded circular ring antenna with semicircular C-shaped radiating slots for multiband applications. The novelty of this paper lies with three techniques as follows: cascading circular rings, semicircular C-shaped slots, and complimentary split ring resonators embedded on the ground are included in the paper. The dimensions with optimised values are $35 \times 35 \times 1.61\,\text{mm}^3$. The antenna operates from 2.124 GHz to 8.284 GHz, and it is deposited on a 1.6 mm thick FR-4 substrate. The radiating patch is built on the substrate; it is made by developing multiple circular ring structures to develop a cascaded ring-like pattern that provides the wideband response. The antenna successfully resonates with a wide bandwidth of 6.16 GHz in the span of 2.124 GHz to 8.284 GHz. The ground features a half hexagonal slot that is embedded within the larger etched rectangular slot. An equivalent circuit with R-L-C elements is developed. The resonating bands are obtained at 3.0 GHz, 5.89 GHz, and 7.07 GHz with reflection coefficients of -21.3 dB, -19.7 dB, and -26.7 dB, respectively. The optimised design operates at UWB, WLAN, WiMAX, and 5G midband applications.

1. INTRODUCTION

In the last decade, wireless communication has gained a lot of attention. The rising demand for the antenna that operates at multiple frequency bands is growing gradually. These days devices are expected to support many services at once, like Wi-Fi, WLAN, and WiMAX, without increasing the dimension and price [1, 2]. This demand for compact antennas increased a bit more, and it gained strong attention in developing multiband and wideband antennas [3, 4]. The conventional design often fails to achieve these requirements. The majority of the designs reported in previous literature work well for single-band applications but fail to cover multiple frequency standards. In other cases, the size of the antenna is large and difficult to fabricate or suffers low impedance matching [5, 6]. Due to these challenges, scientists try to explore new designs with suitable dimensions that can cover wide bandwidth and have good impedance and achieve multiple bands with small dimensions.

Circle-shaped antennas are one of the phenomenal choices due to their wide radiation characteristics and smaller dimension [5]. When circular ring antennas are arranged one into the other, it introduces multiple new resonant paths which improve the efficiency and bandwidth. Also, developing etched slots, particularly improve the like C-shaped slots, can greatly influence the surface currents and also be helpful in supporting additional operating frequencies [7, 8]. On the other hand, complementary split ring resonators are also helpful in enhancing the impedance behaviour of the antenna [9, 10]. A study reported in [11] investigated a ring resonator antenna included with slots having T-shaped stubs developed on the radiating patch and on the ground plane useful in achieving different applications. Ref. [12] illustrates a quadrangular patch having T-shaped slots, and an optimised ground plane achieves a good bandwidth around 77.4% over 5.53 GHz to 12 GHz. Another piece of literature [13], a kite-shaped antenna for UWB applications, achieves a wide bandwidth of 14.2 GHz from 2.8 GHz to 17 GHz. In [14], a T-stub is introduced for an open slot antenna, which improves the bandwidth. In [15, 16], another T-shaped patch antenna developed for wireless applications is introduced. A compact UWB antenna with a transmission feed that covers multiple wireless standards is reported in [17]. In another study [18], a microstrip patch with T-shaped slots improves the performance of the design. An asymmetric U-shaped antenna design with a T-shaped strip, developed with WLAN, WiMAX, and Bluetooth applications, is discussed in [19]. Another study [20] demonstrates a square-shaped ring-based antenna designed for polarisation, and it shows the importance of associating a T-shaped feeding structure. A wideband antenna

* Corresponding author: Kottapadikal Vinodan Vineetha (vineethaammu72@gmail.com).

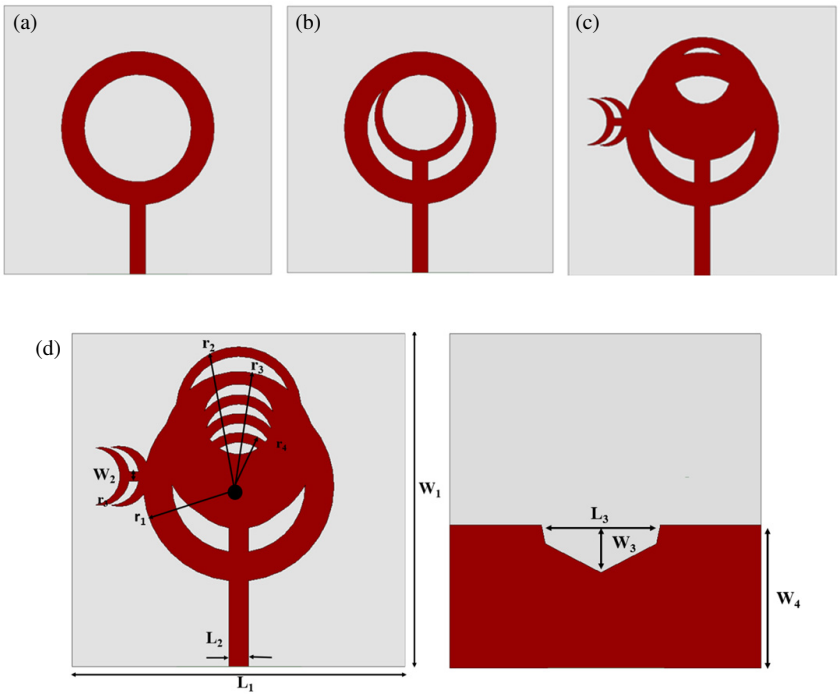

FIGURE 1. Step by step evolution of the SIERS design from initial structure Step 1 to final configuration (Step 1–Step 4).

operating between 1 and 2.5 GHz does not achieve enough bandwidth for the data resolution reported in [21]. A 3D antenna with large dimensions and low gain operating over 1–2.5 GHz is discussed in [22]. A Vivaldi antenna is reported in [23]. It has low gain and bandwidth, unsuitable for medical imaging. Recent literature reports that bandwidth unsuitable for medical imaging is reported in [24]. Circular patch antennas with multiple slots are given in [25–30].

The antenna design is developed using a compact cascaded circular ring structure combined with C-shaped slots to achieve multiband performance. The radiating patch is created by arranging several concentric circular rings, where the cascaded geometry enhances bandwidth and improves radiation behaviour. To further optimise performance, the ground plane is modified with a circular slot, which strengthens impedance matching and supports stable resonances. The antenna covers a wide frequency range from 2.124 GHz to 8.284 GHz, offering an overall bandwidth of 6.16 GHz. Strong resonant modes are observed at 3.0 GHz, 5.89 GHz, and 7.07 GHz, with reflection coefficients of −22 dB, −20 dB, and −28 dB, confirming efficient radiation. Owing to its wideband and multiband response, this antenna is well suited for modern applications like wireless communication, Wi-Fi, radar sensing, satellite connectivity, and emerging IoT systems.

2. GEOMETRY AND DESIGN METHODOLOGY

A cascaded circular annular ring structure associated with C-shaped slots works at multiple frequency bands. The overall dimension of the antenna is small, and it is around nearly $35 \times 35 \times 1.6\,\text{mm}^3$ designed on an FR-4 substrate with a thickness of 1.6 mm. The patch element is developed by arranging several rings, one circular ring inside the other ring. This kind of arrangement enhances the radiation phenomenon and allows the antenna to cover a wider frequency range. Furthermore, to improve the performance, the ground plane of the design is etched with partial hexagon shape. Also, two crescent shape strips are attached on the left-hand side of the antenna. Inside the large rectangular slot, it is etched with a half hexagonal slot. This kind of etched pattern enhances impedance matching and attains multiband response. The circle-shaped annular ring C slotted antenna is fabricated. During the test phase of the device, it shows strong resonance with good reflection coefficients. The obtained reflection coefficient values indicate that antenna radiates effectively at the corresponding resonances. Overall, the design is developed step by step (as it is given in Figure 1) started from basic circular ring patch to the cascaded ring slots until they receive the final desired band. Figure 2 states the prototype model of the proposed antenna with vector network analyser result in an anechoic chamber.

Even though circular ring antennas with C-shaped slots are common usual structures, the novelty of this work relies on integrating three techniques, firstly a cascaded multiple-ring radiator, second one semicircular C-shaped slot loaded on the left side of the patch, and a semi-hexagonal partial etched portion on ground. Integrating this configuration has not been discussed in earlier designs. All these parameters make the proposed design better and produce a much wider bandwidth than conventional circular slot patch antenna designs. All the elements considered in this work are common but coordinating and integrating all of them together make the design unique and lead to significant performance.

This plot shows the reflection coefficient (S_{11}) for different values of the parameter r_1. Small changes in r_1 slightly shift

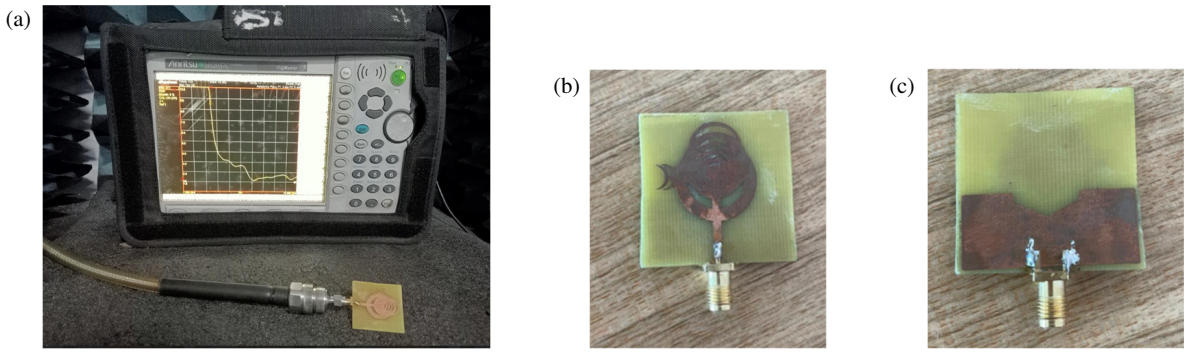

FIGURE 2. (a) Antenna connected with network analyser, (b) fabricated device with connector (front view), (c) fabricated device with connector back view.

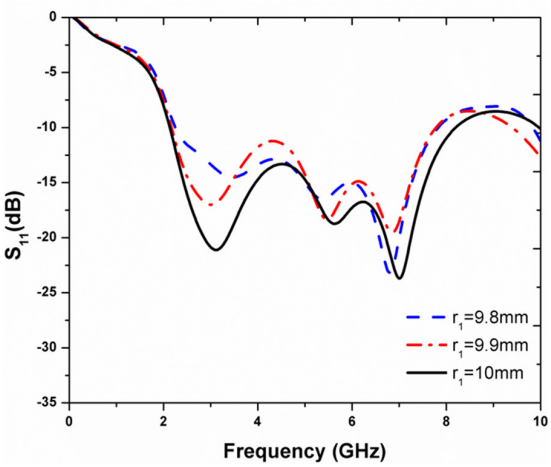

FIGURE 3. S_{11} response for different values of r_1.

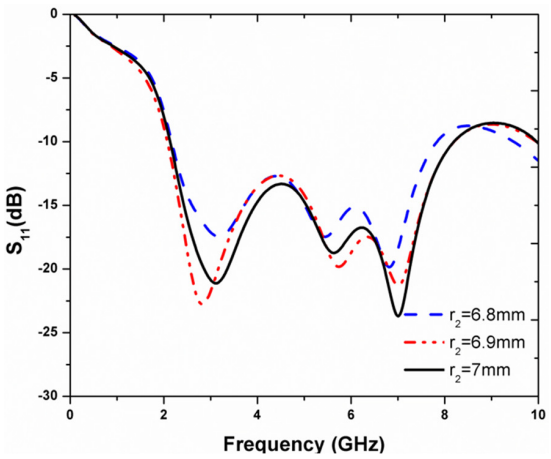

FIGURE 4. S_{11} response for different values of r_2.

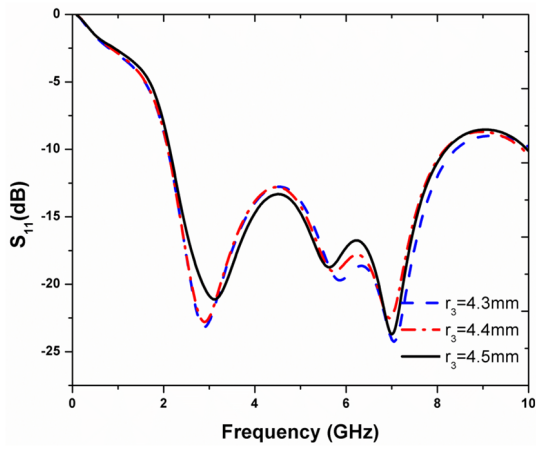

FIGURE 5. S_{11} response for different values of r_3.

the resonant frequencies, but the antenna still maintains good matching across the band. Here, the reflection coefficient is observed for variations in r_2. Just like in Figure 3, the resonant dips shift depending on the radius, showing the antenna's sensitivity to geometric changes. This graph presents the reflection coefficient for different r_3 values. The results again highlight that small dimensional variations impact resonance, but overall wideband behaviour is maintained. This plot illustrates the small variation of r_1 effects on the antenna performance. Small variations in this parameter are sufficient to displace the antennas resonance points, indicating that its sensitivity to the dimensions is extremely high. These bands are different, but the antenna still has more than one resonant band, which demonstrates that the antenna can achieve wideband operation. Here, parameter r_2 is tuned, and S_{11} is plotted in Figure 4. The curves demonstrate that the resonant dips are shifted up and down along the frequency axis with altering r_2 slightly. It implies that r_2 to adjust the tuning frequencies is what really matters, while broadband behaviour persists. Figure 6 shows the effect of r_3 in the return loss of the antenna. As in the other cases, frequency shifts verify dependence on geometrical parameters of the design. The total wideband nature of the antenna is, however, maintained, and it can be seen that the design is robust to changes in r_3 from Figure 5.

These equations explain how the effective radius are determined by taking into account the ring-shaped geometry. With these parameters, the resonant frequency of the antenna is finally obtained through the expressions given in Equations (1)–(13) in [31]. The specifications of the circular ring slotted antenna are shown in Table 1.

$$\varepsilon_{eff} = \frac{\varepsilon_r + 1}{2} + \frac{\varepsilon_r - 1}{2}\left(1 + 12\frac{h}{w}\right)^{1/2} \quad (1)$$

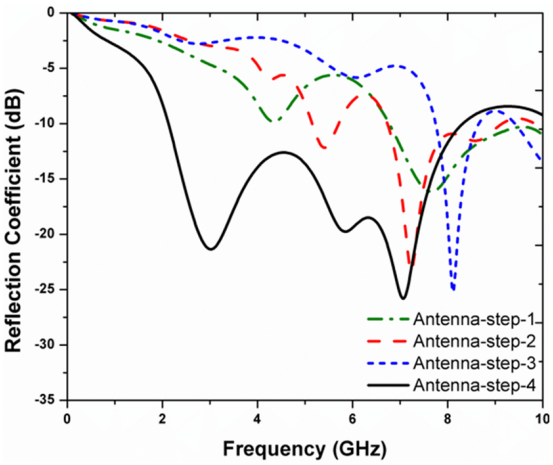

FIGURE 6. Step wise comparison of the antenna design for improvement.

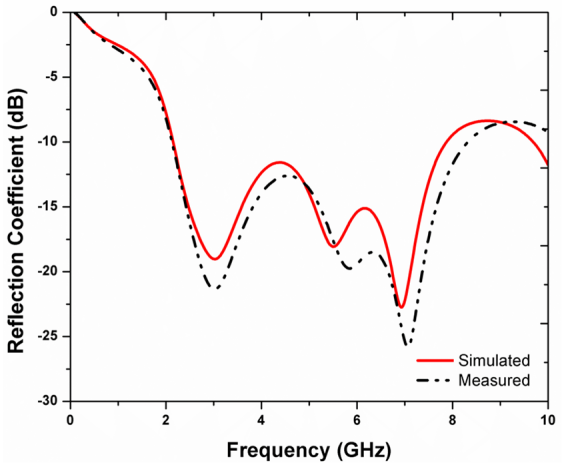

FIGURE 7. Simulated and measured results comparison based on S_{11} performance.

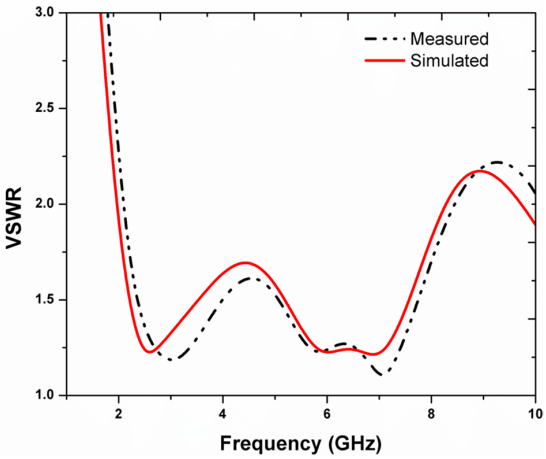

FIGURE 8. Measured VSWR performance of the antenna.

c = speed of the light, and effective radius is calculated by choosing the average of concentric rings.

$$\lambda_0 = \frac{c}{f} \tag{2}$$

Guided wavelength is given as

$$\lambda_g = \frac{\lambda_0}{\sqrt{\varepsilon_{eff}}} \tag{3}$$

Outer slot, middle slot, inner slot radius are calculated using the following equation. Effective slot radius is measured by using (4)

$$r_{eff} = \frac{\lambda_g}{2\pi} \tag{4}$$

Circular annular ring slot radius is measured using the following equation.

$$2\pi r_{eff} \approx n\lambda_g \quad \text{where } n = 1, 2, \ldots \tag{5}$$

TABLE 1. Specifications of the design.

Dimension	Value (mm)	Dimension	Value (μm)
L_1	35	r_4	5
W_1	35	W_2	0.5
L_2	2	W_3	5
r_1	10	W_4	15
r_2	8	L_3	13.7
r_3	6.57		

r_{eff} — effective radius of the circular cascaded slot. Length for semicircular C-shaped slot mean radius r_m and arc angle θ

$$\text{Arclength} \approx r_m\theta = \frac{p\lambda_g}{2} \tag{6}$$

Resonance mode number (an integer, $p = 1, 2, 3, \ldots$) represents the number of half-wavelengths fitting along the slot arc.

Reflection coefficient is approximated by using equation given below

$$\tau = \frac{Z_{in} - Z_0}{Z_{in} + Z_0} \tag{7}$$

$$S_{11}\,(\text{dB}) = 20\log_{10}|\tau| \tag{8}$$

Z_{in} = Input impedance, Z_0 = ref impedance. VSWR is evaluated using equation below

$$\text{VSWR} = \frac{1 + |\tau|}{1 - |\tau|} \tag{9}$$

Fractional bandwidth is evaluated using following equation.

$$\text{FBW} = \frac{f_H - f_L}{f_c} \tag{10}$$

$$f_c = \frac{f_H + f_L}{2} \tag{11}$$

Total efficiency is evaluated using following equation

$$\eta_{tot} = \left(1 - |\tau|^2\right)\eta_{rad} \tag{12}$$

$$\eta_{rad} = \frac{P_{rad}}{P_{acc}} \tag{13}$$

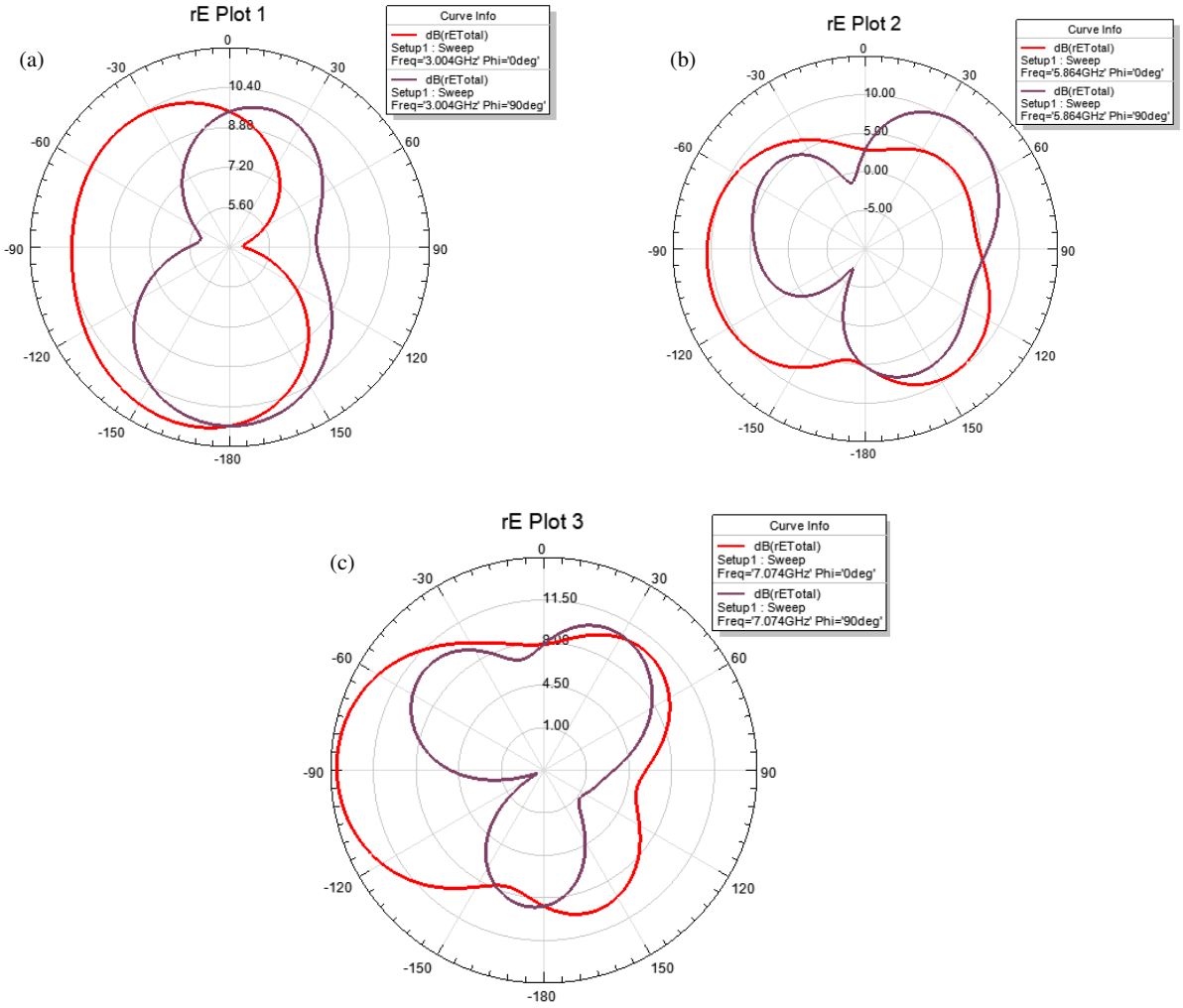

FIGURE 9. Analysing radiation plots at (a) 3.004 GHz, (b) 5.86 GHz, (c) 7.07 GHz.

3. RESULTS AND DISCUSSION

The step-by-step fabrication process of the antenna is illustrated in Figure 6. The effect of design evolution on the antenna's return loss (S_{11}) is shown in Figure 3, where each curve corresponds to a different stage (Step-1 to Step-4). The sharp dips in the curves indicate strong impedance matching at those frequencies. In Figure 7, the simulated and measured return losses of the final design are compared. The simulated response is shown in black, while the measured one is shown in red. The close agreement between the two confirms that the fabricated antenna performs very similarly to its simulated model. Finally, Figure 8 presents the voltage standing wave ratio (VSWR) for both simulated and measured cases. A VSWR value approaching 1 represents good impedance matching, and the close overlap of the two curves demonstrates that the antenna achieves reliable performance in practice.

The shapes of the lobes show how the antenna radiates at different bands, and they confirm that the antenna maintains directional radiation with stable performance, as shown in Figure 9. This plot shows the antenna gain versus frequency. Simulated and measured results are closely matched, with gain (Figure 10) values staying around 5–6 dB, which is considered good for practical applications. This figure shows the radiation efficiency (Figure 11) of the antenna across frequency. The efficiency remains high (above 70% for most of the band), with good agreement between simulated and measured data.

These surface currents in Figure 12 explain how the current changes on the antenna at different operating bands. The currents majorly located around the feed and central ring, highlighted with yellow and green colour. When the frequency increases, stronger currents appear highlighted with red colour. The upper portion of the antenna and C-shaped side slots gradually step by step become much active, indicating most parts of the antenna ready to contribute to radiation. The current spreads widely across the antenna structure, explaining that the antenna is fully activated at all the operating frequencies and initiates multi-band characteristic by activating different parts at different frequencies.

The corresponding lumped-element model used to depict the multi-resonant behaviour of the suggested structure is shown in Figure 13. A 50-Ω source feeds a cascaded series network with three resistive sections (50 Ω, 40 Ω, and 30 Ω) that allow isolation and control over the total loaded quality factor. A shunt series L-C resonator is linked to ground at each node in between these resistive segments. At their respective resonant

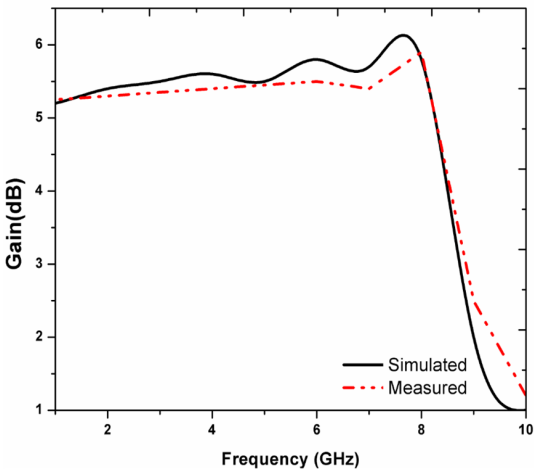

FIGURE 10. Gain of the design across frequency.

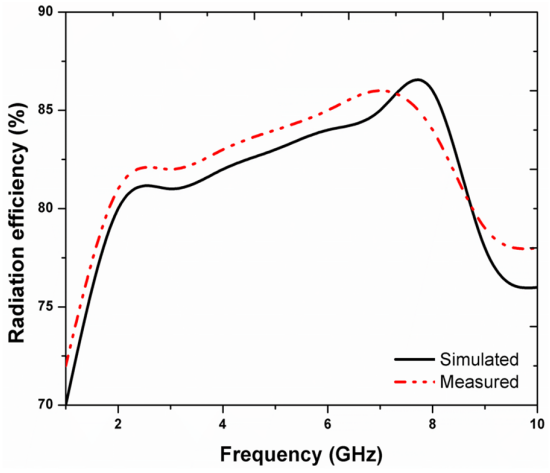

FIGURE 11. Radiation efficiency of the design across the frequency.

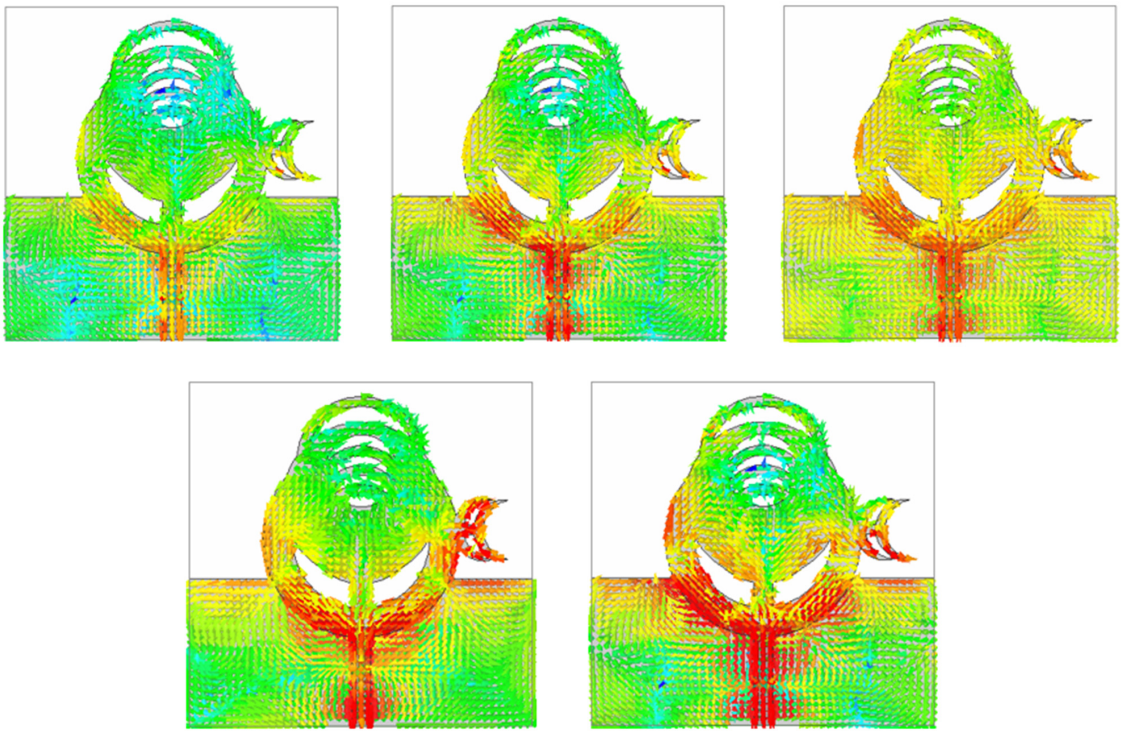

FIGURE 12. Current flows on the antenna at different three operating frequencies and nearby frequencies to show the variation.

frequencies, the first resonator (1 nH/2 pF), second resonator (0.4 nH/1 pF), and third resonator (0.33 nH/1 pF) all provide a series resonance path that effectively presents a low impedance. The shunt L-C branch briefly acts as a short to ground when resonance takes place, creating a steep attenuation (notch) in the gearbox path. The signal can flow through the series chain because the shunt branches have high impedance when they are not in resonance. As a result, this stepped architecture simulates a three-notch band-stop response, with each notch's depth and bandwidth determined by the resonators' L-C values and series resistances.

The current fields spread over nearly the entire patch and ground plane, indicating that most of the area is helpful in circulating radiation. At the high operating frequencies, all currents are accumulated near the slots and edges of the patch. This demonstrates that those areas are solely responsible for resonance. In a way, current changes with frequency prove that the antenna operates in several resonant bands, suitable for wideband applications. These fields explain how different parts of the antenna get activated, as shown in Figure 12. This provides stable performance at different bands. The comparison in Table 2 also makes it clear that this design is both compact in size and able to achieve a wide bandwidth of 6.16 GHz. Along with that, it maintains good gain across the bands, which makes it more efficient than many earlier antenna designs for today's wireless systems.

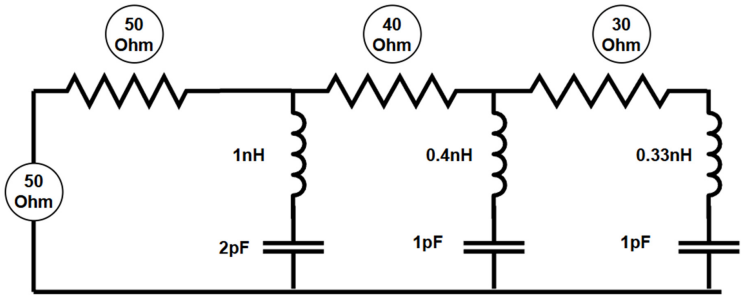

FIGURE 13. RLC circuit of the proposed antenna.

TABLE 2. Performance comparison with other designs in literature.

Reference	Antenna Size (λ)	Operating Bands (GHz)	Achieved Bandwidth (GHz)	Peak Gain (dBi)
[23]	$2 \times 2 \times 1.2$	2.17–2.72 3.34–3.66 4.85–5.77	0.55 0.32 0.92	3.75 3.56 3.93
[19]	$0.75 \times 1.625 \times 0.04$	2.375–2.525 3.075–3.80 5.00–6.90	0.15 0.725 1.9	1.30 5.20 3.10
[20]	$1.66 \times 1.16 \times 0.023$	1.68–2.04 3.05–4.1 7.62–8.42	0.36 1.05 0.8	5
[22]	$0.18 \times 0.14 \times 0.01$	2.09–2.64	0.55	4.5
[29]	$0.7 \times 0.54 \times 0.032$	1.96–2.22 3.51–3.91 4.78–5.26	0.26 0.4 0.48	5
[26]	$0.6 \times 0.6 \times 0.015$	2.12–2.28	0.16	5.3
Proposed antenna	$1.16 \times 1.16 \times 0.023$	3.0 5.89 7.07 2.124–8.284	6.16	2.6 4.6 7.2

4. CONCLUSION

This work presents a compact antenna design based on cascaded circular rings combined with C-shaped slots. The use of multiple rings and a half-hexagonal slot in the ground helps the antenna operate over a wide range of frequencies. The measured resonances at 3.0 GHz, 5.89 GHz, and 7.07 GHz confirm its efficiency across different bands. Built on an FR-4 substrate with optimised dimensions, the antenna is both small in size and practical for real-world use. The overall study shows that this structure improves bandwidth, ensures better impedance matching, and delivers a dependable multiband response for modern wireless communication needs. The covered range also includes important practical standards such as WLAN (2.4, 5.2, and 5.8 GHz), WiMAX (3.5 and 5.5 GHz), 5G mid-band (3.3–4.2 GHz and 4.4–5.0 GHz), and UWB (3.1–8 GHz).

REFERENCES

[1] Khan, M. U., M. S. Sharawi, and R. Mittra, "Microstrip patch antenna miniaturisation techniques: A review," *IET Microwaves, Antennas & Propagation*, Vol. 9, No. 9, 913–922, 2015.

[2] Lee, K.-F. and K.-F. Tong, "Microstrip patch antennas-basic characteristics and some recent advances," *Proceedings of the IEEE*, Vol. 100, No. 7, 2169–2180, Jul. 2012.

[3] Al-Amoudi, M. A., "Study, design, and simulation for microstrip patch antenna," *International Journal of Applied Science and Engineering Review (IJASER)*, Vol. 2, No. 2, 1–29, 2021.

[4] Altufaili, M. M. S., A. N. Najaf, and Z. S. Idan, "Design of circular-shaped microstrip patch antenna for 5G applications," *TELKOMNIKA (Telecommunication Computing Electronics and Control)*, Vol. 20, No. 1, 19–26, 2022.

[5] Deng, C., Z. Zhao, and W. Yu, "Characteristic mode analysis of circular microstrip patch antenna and its application to pattern diversity design," *IEEE Access*, Vol. 10, 2399–2407, 2021.

[6] Mukta, C., M. Rahman, and A. Z. M. T. Islam, "Design of a compact circular microstrip patch antenna for WLAN applications," *International Journal on AdHoc Networking Systems*, Vol. 11, No. 3, 1–11, 2021.

[7] Thaher, R. H. and L. M. Nori, "Design and analysis of multiband circular microstrip patch antenna for wireless communication," *Periodicals of Engineering and Natural Sciences*, Vol. 10, No. 3, 23–30, 2022.

[8] Muthuvel, S. K., M. Shaw, and Y. K. Choukiker, "Concentric circular compound reconfigurable microstrip patch antenna for wireless applications," *AEU — International Journal of Electronics and Communications*, Vol. 141, 153960, 2021.

[9] Ayalew, L. G. and F. M. Asmare, "Design and optimization of pi-slotted dual-band rectangular microstrip patch antenna using surface response methodology for 5G applications," *Heliyon*, Vol. 8, No. 12, e12030, 2022.

[10] Sabila, L. Y., A. Yudhana, M. M. Amri, A. Akrima, and I. P. Pratama, "Design of circular patch array microstrip antenna using slot for ISM band," *Journal of Electrical Technology UMY*, Vol. 6, No. 2, 77–84, 2022.

[11] Da Xu, K., Y. H. Zhang, R. J. Spiegel, Y. Fan, W. T. Joines, and Q. H. Liu, "Design of a stub-loaded ring-resonator slot for antenna applications," *IEEE Transactions on Antennas and Propagation*, Vol. 63, No. 2, 517–524, Feb. 2015.

[12] Yadav, N. P., M. R. Tripathy, and Y. Jeong, "T-shaped slot loaded rectangular patch antenna with enhanced bandwidth using defected ground structure," in *2018 Progress In Electromagnetics Research Symposium (PIERS-Toyama)*, 1570–1575, Toyama, Japan, 2018.

[13] Tiwari, R. N., P. Singh, B. K. Kanaujia, and A. K. Pandit, "A coalesced kite shaped monopole antenna for UWB technology," *Wireless Personal Communications*, Vol. 114, No. 4, 3031–3048, 2020.

[14] Song, K., Y.-Z. Yin, X.-B. Wu, and L. Zhang, "Bandwidth enhancement of open slot antenna with a T-shaped stub," *Microwave and Optical Technology Letters*, Vol. 52, No. 2, 390–393, 2010.

[15] Verma, R. K. and D. K. Srivastava, "Bandwidth enhancement of a slot loaded T-shape patch antenna," *Journal of Computational Electronics*, Vol. 18, No. 1, 205–210, 2019.

[16] Ansari, J. A. and S. Verma, "Analysis of T-slot loaded disk patch antenna for dual band operation with small frequency ratio," *International Journal of Future Generation Communication and Networking*, Vol. 8, No. 3, 15–30, 2015.

[17] Tiwari, R. N., P. Singh, and B. K. Kanaujia, "A modified microstrip line fed compact UWB antenna for WiMAX/ISM/WLAN and wireless communications," *AEU — International Journal of Electronics and Communications*, Vol. 104, 58–65, 2019.

[18] Sharma, A., B. K. Kanaujia, and S. Kumar, "Compact microstrip antenna loaded with T-shaped slots," in *2013 International Conference on Microwave and Photonics (ICMAP)*, 1–3, Dhanbad, India, 2013.

[19] Tiwari, R. N., P. Singh, and B. K. Kanaujia, "Asymmetric U-shaped printed monopole antenna embedded with T-shaped strip for Bluetooth, WLAN/WiMAX applications," *Wireless Networks*, Vol. 26, No. 1, 51–61, 2020.

[20] Sung, Y., "Stub-loaded square-ring antenna for circular polarization applications," *Journal of Electromagnetic Waves and Applications*, Vol. 30, No. 11, 1465–1473, 2016.

[21] Ruvio, G., M. J. Ammann, M. John, R. Solimene, A. D'Alterio, and R. Pierri, "UWB breast cancer detection with numerical phantom and Vivaldi antenna," in *2011 IEEE International Conference on Ultra-Wideband (ICUWB)*, 8–11, Bologna, Italy, 2011.

[22] Mobashsher, A. T., K. S. Bialkowski, and A. M. Abbosh, "Design of compact cross-fed three-dimensional slot-loaded antenna and its application in wideband head imaging system," *IEEE Antennas and Wireless Propagation Letters*, Vol. 15, 1856–1860, 2016.

[23] Salleh, A., C. C. Yang, M. S. J. Singh, and M. T. Islam, "Development of antipodal Vivaldi antenna for microwave brain stroke imaging system," *International Journal of Engineering & Technology*, Vol. 8, No. 3, 162–168, 2019.

[24] Alqadami, A. S. M., N. Nguyen-Trong, B. Mohammed, A. E. Stancombe, M. T. Heitzmann, and A. Abbosh, "Compact unidirectional conformal antenna based on flexible high-permittivity custom-made substrate for wearable wideband electromagnetic head imaging system," *IEEE Transactions on Antennas and Propagation*, Vol. 68, No. 1, 183–194, Jan. 2020.

[25] Zainud-Deen, S. H., N. A. El-Shalaby, H. A. Malhat, and S. M. Gaber, "Reconfigurable multi-turns planar plasma helical antenna," *Plasmonics*, Vol. 14, No. 6, 1831–1837, 2019.

[26] Babu, G. H., M. Srinivas, C. Gnanaprakasam, R. T. Prabu, M. R. Devi, S. H. Ahammad, M. A. Hossain, and A. N. Z. Rashed, "Meander line base asymmetric co-planar wave guide (CPW) feed tri-mode antenna for Wi-Max, North American Public Safety and satellite applications," *Plasmonics*, Vol. 18, No. 3, 1007–1018, 2023.

[27] Bag, B., P. Biswas, R. Mondal, S. Biswas, and P. P. Sarkar, "Circularly polarized quad-band monopole antenna of wireless communication system," *International Journal of RF and Microwave Computer-Aided Engineering*, Vol. 29, No. 9, e21818, 2019.

[28] Shaw, M., N. Mandal, and M. Gangopadhyay, "A compact circularly polarized isosceles triangular microstrip patch antenna with parasitic elements for multiband application," *Microwave and Optical Technology Letters*, Vol. 62, No. 10, 3275–3282, 2020.

[29] Nallapaneni, S. and P. Muthusamy, "Design of multiband fractal antenna loaded with parasitic elements for gain enhancement," *International Journal of RF and Microwave Computer-Aided Engineering*, Vol. 31, No. 6, e22622, 2021.

[30] Shinde, J. P., R. Kumar, and M. D. Uplane, "Circular polarization in defected hexagonal shaped microstrip antenna," *Wireless Personal Communications*, Vol. 75, No. 2, 843–856, 2014.

[31] Balanis, C. A., *Antenna Theory: Analysis and Design*, John Wiley & Sons, 2016.